REPORT

APPLIED PHYSICS

Monolithic optical microlithography of high-density elastic circuits

Yu-Qing Zheng[1]†, Yuxin Liu[2]†, Donglai Zhong[1]†, Shayla Nikzad[1], Shuhan Liu[1], Zhiao Yu[1,3], Deyu Liu[1], Hung-Chin Wu[1], Chenxin Zhu[1], Jinxing Li[1], Helen Tran[1], Jeffrey B.-H. Tok[1], Zhenan Bao[1]*

Polymeric electronic materials have enabled soft and stretchable electronics. However, the lack of a universal micro/nanofabrication method for skin-like and elastic circuits results in low device density and limited parallel signal recording and processing ability relative to silicon-based devices. We present a monolithic optical microlithographic process that directly micropatterns a set of elastic electronic materials by sequential ultraviolet light–triggered solubility modulation. We fabricated transistors with channel lengths of 2 micrometers at a density of 42,000 transistors per square centimeter. We fabricated elastic circuits including an XOR gate and a half adder, both of which are essential components for an arithmetic logic unit. Our process offers a route to realize wafer-level fabrication of complex, high-density, and multilayered elastic circuits with performance rivaling that of their rigid counterparts.

Skin-like and elastic electronics that conform to biological tissue and accommodate body movements are ideal for on-skin sensors (*1*–*3*), body area networks (*4*, *5*), and implantable bioelectronics (*6*, *7*). Relative to conventional rigid electronics, such as silicon-based devices, elastic electronics are currently limited with respect to parallel signal recording and processing because of low device density. Therefore, bio-integrated electronics typically adopt a hybrid approach of integrating rigid and stretchable parts (*8*–*10*), but this hybrid approach results in localized stress at rigid-soft interfaces and mismatch in mechanical properties when in contact with biological systems. To construct fully elastic sensing systems, rigid chips in direct contact with biological systems should be replaced by elastic ones. The main limitation to making dense circuits is the lack of scalable patterning methods for polymeric electronic materials, especially for micro/nanopatterning soft and elastic electronic materials into complex, high-density, multilayered functional devices and circuits (*11*–*13*).

A staple technique in the silicon-based semiconductor industry, photolithography, has successfully enabled shrinking of the channel length of silicon transistors down to the nanometer scale, thus allowing highly integrated circuit fabrication. Unfortunately, conventional photolithography does not accommodate micro/nanofabrication of polymeric electronic materials (e.g., semiconductors and conductors) because the photoresists used in photolithography lack chemical orthogonality with active polymeric electronic materials (*14*, *15*). Although solution processing of polymeric materials allows ease of fabrication at low production cost (such as screen or inkjet printing), these are low-density patterning techniques with spatial resolution of hundreds of micrometers (*16*–*18*).

To address these limitations, we describe a monolithic optical microlithographic process (termed PhotoAssist) for high-density production of elastic circuits. This process involves direct optical lithography on polymeric electronic materials (Fig. 1, A to D). We took advantage of both the post-functionalization property of polymeric materials and the benefits of traditional photolithography, including high spatial resolution and low cost per patterned element. PhotoAssist directly patterns multiple electroactive materials via a sequence of ultraviolet (UV) light exposures without the need for photoresist and stripping processes. Specifically, we used an efficient light-triggered carbene insertion reaction as a general crosslinking method for semiconducting polymers and insulating polymers (Fig. 1E). In addition, we introduced UV-sensitive polyethylene glycol dimethacrylate (PEGDMA) to realize double network–mediated direct optical lithography of a chemically unmodified conducting polymer. All our polymer-based transparent elastic electronics were fabricated through only four steps of direct optical microlithography, without the need for additional protection, etching, transfer, or lamination processes (Fig. 1F). The crosslinking-based patterning strategy enabled robust immobilization of each layer and chemical resistance, thus enabling layer-by-layer sequential deposition at wafer scale.

Typical conducting polymers such as poly(3,4-ethylenedioxythiophene) polystyrene sulfonate (PEDOT:PSS) have limited reaction sites for direct covalent crosslinking. Therefore, we used a "double network" physical crosslinking strategy for direct optical lithography to pattern PEDOT:PSS with high spatial resolution. We hypothesized that solubility modulation of PEDOT:PSS can be realized through embedding of a physical crosslinked conductive network into a covalently crosslinkable PEGDMA network. We observed that the strong interaction between PEDOT and PEG linker resulted in a microstructure transition of PEDOT:PSS from a core-shell structure into more extended chains, thus forming the first conductive network (Fig. 2A). After UV light (365 nm) initiation, the dimethyl acrylate (DMA)–modified PEG undergoes a rapid radical polymerization to form the second network. The strong intermolecular interaction between the two networks enabled the UV-exposed regions to be resistant to subsequent water development, whereas the UV-unexposed regions remained water-soluble.

We observed that the photopatternability is highly dependent on the PEGDMA/PEDOT weight ratio, which needs to be in the range 1.10:1 to 1.58:1 (Fig. 2B and supplementary text). Films with insufficient PEGDMA (<1.10:1 versus PEDOT) did not become insoluble against developer, whereas excessive PEGDMA (>1.58:1 versus PEDOT) led to undesirable physical crosslinking before UV exposure. With the addition of more PEG linkers, the PEDOT π-π stacking distance gradually decreased and larger crystallites were formed as a result of the stronger interchain coupling between PEDOT molecules (Fig. 2, C and D, and figs. S2 and S3). Atomic force microscopy images confirmed that when 1.10:1 PEGDMA/PEDOT was added to PEDOT:PSS, the morphology of PEDOT:PSS changed from a featureless film (fig. S4) to interconnected PEDOT fibers. Such microstructure change confirms that a physically crosslinked PEDOT network with denser packing can be retained within a secondary chemically crosslinked PEG network formed under UV, endowing the system with UV-modulated solubility (fig. S5). By mixing 1.15:1 PEGDMA/PEDOT and 5% weight ratio of water-soluble initiator versus PEGDMA, we achieved a negative PEDOT:PSS pattern after UV light (365 nm) exposure and subsequent development with water. High-resolution PEDOT:PSS patterns with feature sizes down to 2 μm, which include fine lines (line width = 2 μm) and narrow gaps between lines (gap width = 2 μm) (Fig. 2, E and F, and figs. S6 and S7), were demonstrated.

Addition of PEGDMA also substantially increased the PEDOT:PSS conductivity; the

[1]Department of Chemical Engineering, Stanford University, Stanford, CA 94305, USA. [2]Department of Bioengineering, Stanford University, Stanford, CA 94305, USA. [3]Department of Chemistry, Stanford University, Stanford, CA 94305, USA.
*Corresponding author. Email: zbao@stanford.edu
†These authors contributed equally to this work.

Downloaded from https://www.science.org at Institute of High Performance Computing on November 24, 2021

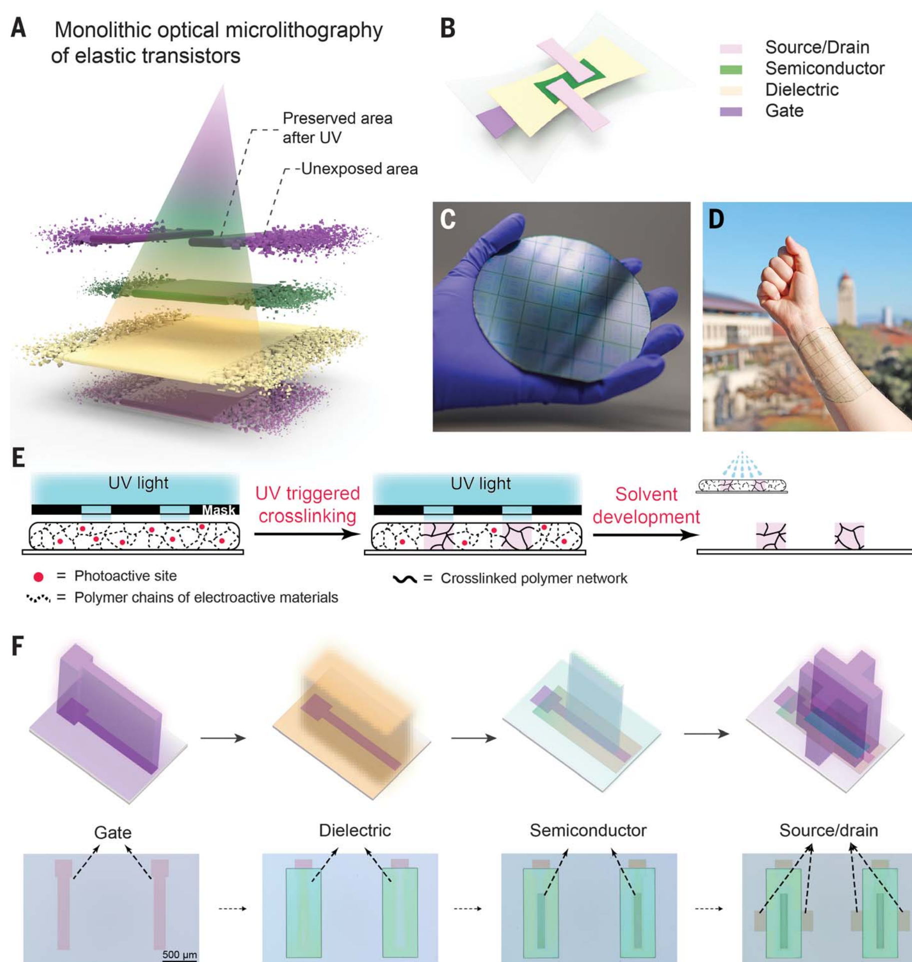

Fig. 1. Monolithic optical microlithography for high-density elastic circuits. (**A**) Schematic illustration of monolithic optical microlithography. Elastic electronic materials are directly patterned sequentially by a series of UV light–triggered solubility modulation processes. The UV-exposed area has substantially reduced solubility and thus is preserved after the solvent development process. (**B**) Device configuration of elastic transistors with bottom gate and top contact. (**C**) Photograph of a 4-inch wafer-scale elastic circuit array fabricated by monolithic optical microlithography. (**D**) Photograph showing appearance of elastic circuit array released from a supportive wafer and attached to a human forearm. (**E**) General mechanism of the PhotoAssist strategy for direct optical lithography of elastic electronic materials based on UV-triggered crosslinking. (**F**) Monolithic optical microlithography process for sequential patterning of each layer in an elastic transistor (top) and optical image for each step (bottom).

Downloaded from https://www.science.org at Institute of High Performance Computing on November 24, 2021

PEDOT formed closer stacking and a more interconnected nanofiber network, and the insulating PSS shell was reduced (Fig. 2G). The conductivity was enhanced from 12.0 ± 3.1 S/m for the original PEDOT:PSS to 3.15 ± 0.68 kS/m for PEDOT:PSS with 1.29:1 PEGDMA/PEDOT. We also observed that methanol treatment further improved the conductivity to 52.5 ± 1.69 kS/m.

Direct optical lithography of both semiconducting and insulating polymers was accomplished by chemical crosslinking via UV-triggered reactions (Fig. 3A). To prevent degradation of the semiconducting polymer charge transport properties, the light-triggered crosslinking reaction needs to be specific to the nonconjugated side chains without breaking the conjugation in the backbone. Inspired by photoaffinity labeling in biological applications (*19*, *20*), we introduced a double-end functionalized trifluoromethyl-substituted diazirine crosslinker (branched-diazirine crosslinker) into the semiconducting polymer films (Fig. 3A). Carbene species formed by rapid photolysis can undergo a clean reaction specific to nonconjugated bonds on side chains of conjugated polymers, leading to increased molecular weight and therefore UV-induced solubility modulation (*21*, *22*). A branched alkyl chain was selected as the linker to reduce crosslinker crystallization and to improve miscibility with semiconducting polymers for efficient photo-crosslinking and greater film deformability (*23*). Carbene generation and reaction could be achieved during UV radiation (365 nm) with a dose of 720 mJ cm^{-2} (figs. S11 and S12). Unchanged positions and integrals of ^1H peaks corresponding to thiophene groups (8.9, 7.7, and 7.3 ppm) in nuclear magnetic resonance spectra suggest that carbene does not react with the π-conjugated core (fig. S13). Instead, the main photo-crosslinking products are from insertion of carbene into nonconjugated C-H bonds, as evidenced by the disappearance of CH_2 (symmetric stretching υ_s = 2854 cm^{-1}; asymmetric stretching υ_{as} = 2926 cm^{-1}) and CH_3 (υ_{as} = 2957 cm^{-1}) in Fourier-transform infrared spectroscopy (Fig. 3C). Therefore, the photoreactions of the branched-diazirine crosslinker are deemed “electronically clean” and are compatible with semiconducting polymer applications. Moreover, activation and decomposition of the branched-diazirine crosslinker occurred at 120°C and >350°C, respectively (figs. S14 and S15), providing a wide processing window for subsequent thermal annealing steps.

Photo-crosslinking efficiency varies with polymer molecular weight (Fig. 3B). Polymers with higher molecular weight and therefore lower initial solubility require a lower crosslinker concentration to achieve full insolubility against the developing solvent. As a representative semiconducting polymer, diketopyrrolopyrrole (DPP)–based conjugated polymer, poly(tetrathienoacene-diketopyrrolopyrrole) (PTDPPTFT4), is used here as a model compound for photo-crosslinking efficiency measurement. We observed that when the molecular weight of the DPP polymer was equal to or higher than 49,000, less than 10 wt% of branched-diazirine crosslinker was needed to realize 99% film retention. Semiconducting polymers containing patterns with feature sizes down to 4 μm were successfully obtained using the carbene-mediated direct optical lithography process (Fig. 3D and fig. S16). The resolution can be further improved by lowering the molecular weight distribution. The branched-diazirine crosslinker was shown to be effective as a general crosslinker that can be used to pattern all common alkylated conjugated

polymers, including poly(3-hexylthiophene) (P3HT), isoindigo-bithiophene semiconducting polymers with carbosilane side chains (PII2T-C6), and an n-type naphthalenediimide (NDI)–based polymer, P(NDI2TOD) (fig. S17).

A crosslinker amount less than 10 wt% is sufficient for achieving good patterning with moderate conjugated polymer molecular weight while maintaining charge transport almost unchanged from that of unpatterned films. Higher crosslinker content led to a decrease in mobility (Fig. 3E and table S1). The polymer aggregation behavior, crystalline domain size, and π-π stacking distances were hardly changed even with as high as 50 wt% of crosslinker versus DPP polymer (figs. S18 to S21 and supplementary text). This result indicates that the branched-diazirine crosslinker selectively interacted with the alkyl chains of the conjugated polymers as a consequence of the chemical structure similarity between the crosslinker and alkyl chains, rather than by interrupting π-stacking between conjugated backbones. Therefore, the decrease in mobility with a large amount of crosslinker may be simply due to the dilution of the semiconducting fraction in the mixture, or to variation in backbone packing orientation (fig. S22).

The carrier mobility of the semiconducting polymer remained unaffected throughout the multiple PhotoAssist steps, including UV exposure and development (fig. S23 and table S2), thanks to the well-preserved conjugated backbone structure and the crystalline microstructures of the conjugated polymers (figs. S24 to S27 and supplementary text). Solvent (chloroform) development showed only a slight decrease in mobility, with average mobility of 0.62 $cm^2 V^{-1} s^{-1}$, indicating good retention of the crosslinked films under solvent development; this is consistent with the gel curve results.

Dielectric polymers can also be directly patterned into different shapes with resolution down to 8 μm by adding 10 wt% of branched-diazirine crosslinker into the system (Fig. 3F and fig. S28). Dielectric properties of poly(methyl methacrylate)–poly(*n*-butyl acrylate)–poly(methyl methacrylate) (PMMA-PnBA-PMMA) and polystyrene-*block*-poly(ethylene-*ran*-butylene)-*block*-polystyrene (SEBS) elastomers showed negligible dependence on UV crosslinking and solvent development steps during the PhotoAssist fabrication processes (Fig. 3G and fig. S29).

Our PhotoAssist methodology is a direct optical lithography applicable to a variety of stretchable electronic materials. Its crosslinking-based mechanism allows the obtained polymer patterns to be resistant against solvents during subsequent processing. Furthermore, electronic properties of all materials remained unaffected, or even improved, after the patterning steps. These properties make PhotoAssist a viable strategy for monolithic manufacturing of high-density elastic electronics. The fabrication process for an elastic transistor array is illustrated in Fig. 1E. The process starts with a sacrificial layer (e.g., dextran) coated onto a Si substrate for eventual device release later. Next, a layer of stretchable elastomer, PMMA-PnBA-PMMA, is deposited, serving as the supporting substrate. The PMMA-PnBA-PMMA elastomer is crosslinked with 10 wt% of branched-diazirine crosslinkers to facilitate subsequent direct deposition of electronic polymer materials without chemical erosion. Next, bottom-gate and top-contact transistors are constructed by consecutive deposition and patterning of a stretchable gate layer (PEDOT:PSS/PEGDMA), a stretchable dielectric layer (PMMA-PnBA-PMMA/branched diazirine), a stretchable semiconductor layer [thieno[3,2-b]thiophene-diketopyrrolopyrrole (DPPTT)/branched diazirine], and a stretchable source/drain layer (PEDOT:PSS/PEGDMA) by direct optical lithography (Fig. 1E and fig. S30). Finally, the fabricated device is released from the supporting Si wafer as a free-standing stretchable electronic device (fig. S31).

We have successfully fabricated an all-polymer elastic transistor array containing 10,000 transistors within a 0.238-cm^2 substrate (Fig. 4, A and B), enabling a device density of ~42,000 transistors/cm^2, more than 100 times the density reported by (*11*), which had involved shadow masking and etching processes. The transistor was designed to have a channel length L_{ch} of

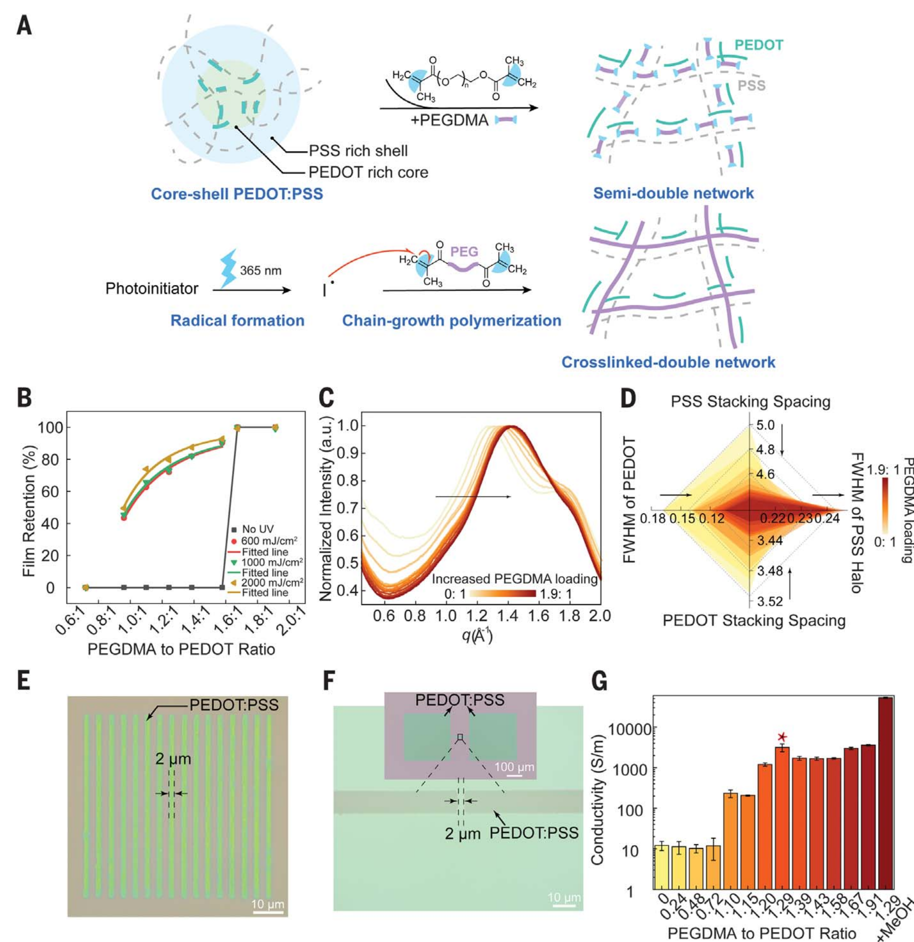

Fig. 2. Double network–mediated direct optical lithography of conductive polymers. (**A**) Mechanism of direct optical lithography of PEDOT:PSS by selective crosslinking of PEGDMA to form a double network that is insoluble in water. (**B**) Gel curves of PEDOT:PSS with different amounts of PEGDMA under different doses of UV exposure. (**C**) Polarization-corrected meridian line cuts from 2D grazing incidence x-ray diffraction (GIXD) for films spin-cast from PEDOT:PSS solutions mixed with different amounts of PEGDMA versus PEDOT. (**D**) Radar chart displaying PSS π-π stacking distance, PEDOT π-π stacking distance, full width at half maximum (FWHM) of PSS scattering halo, and FWHM of PEDOT scattering halo determined from GIXD of UV-exposed PEDOT:PSS/PEGDMA films. (**E**) Optical image of a representative PEDOT:PSS fine line pattern with 2-μm resolution by direct optical lithography. (**F**) Optical image of a PEDOT:PSS pattern with a 2-μm gap by direct optical lithography. (**G**) Dependence of UV-exposed PEDOT:PSS/PEGDMA film conductivity on proportion of PEGDMA. Error bars denote SD. The sample marked as 1.29+MeOH is with 1.29:1 weight ratio of PEGDMA versus PEDOT and is treated with methanol after crosslinking.

Downloaded from https://www.science.org at Institute of High Performance Computing on November 24, 2021

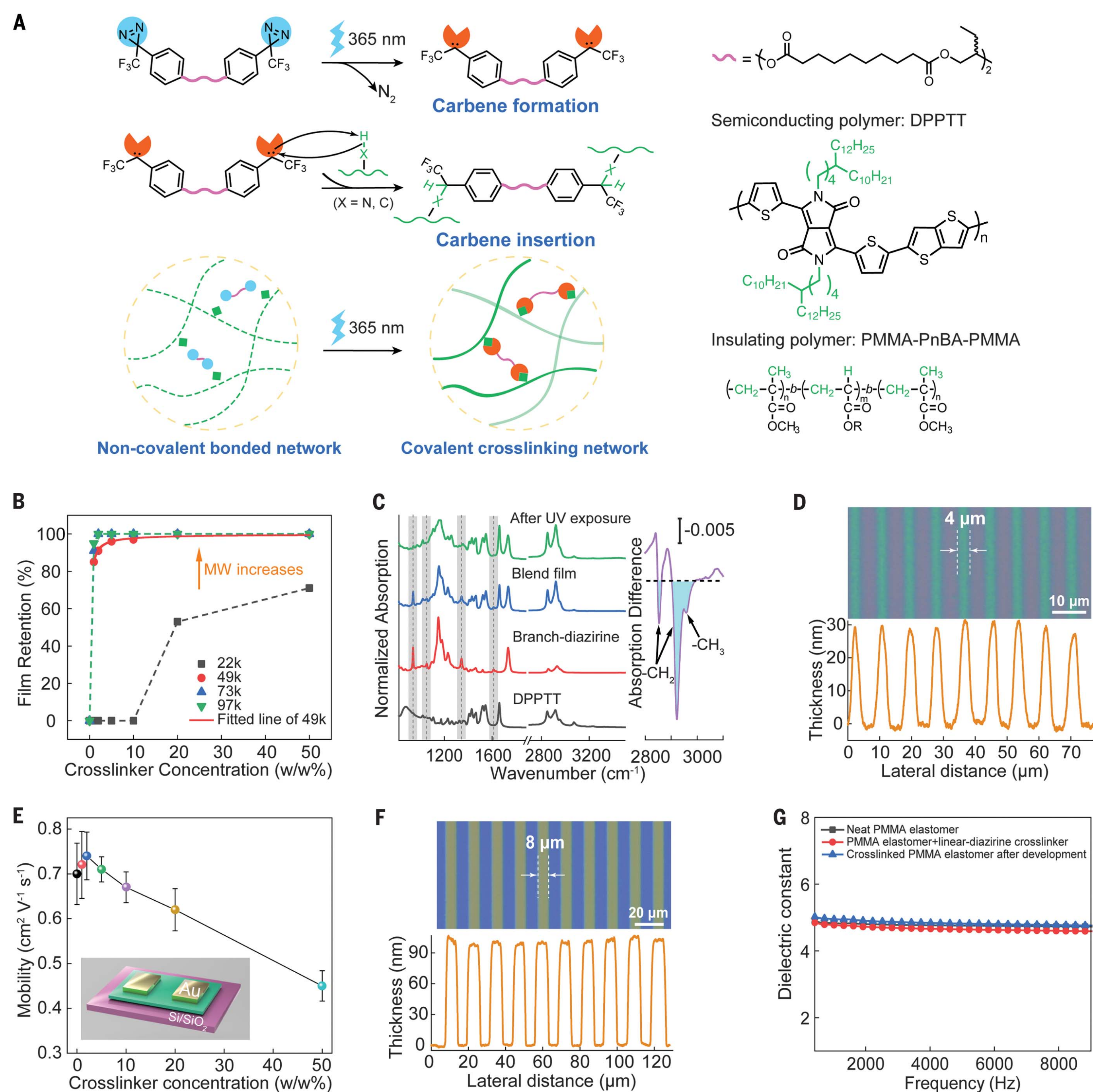

Fig. 3. Carbene-mediated direct optical lithography of semiconducting and insulating polymers. (**A**) Mechanism of direct optical lithography for semiconducting and dielectric polymers based on UV-triggered carbene insertion crosslinking. (**B**) Gel curves of representative semiconducting DPP polymer with different molecular weights mixed with different amounts of branched-diazirine crosslinker (0, 1, 2, 5, 10, 20, and 50 wt% versus DPP polymer) under different doses of UV exposure. Film retention percentage is the ratio of crosslinked film thickness before developing versus after developing. (**C**) Left: Fourier-transform infrared spectrum of neat DPPTT, neat branched-diazirine crosslinker, DPPTT with 20 wt% of branched-diazirine crosslinker blend, and UV-crosslinked blend. Right: Photoreaction spectra obtained as the difference before and after UV exposure, showing branched-diazirine reaction with $-CH_2$ and $-CH_3$ groups. (**D**) Top: Optical image of DPPTT fine line pattern with 4-μm resolution by direct optical lithography. Bottom: Height profile of DPPTT polymer pattern obtained from PhotoAssist. (**E**) Average mobility of crosslinked polymer films containing different amounts of branched-diazirine crosslinker. Error bars denote SD. Inset: Schematic of OFET device fabricated on OTS-modified SiO_2/Si. (**F**) Top: Optical image of PMMA-PnBA-PMMA elastomer pattern with 8-μm resolution by direct optical lithography. Bottom: Height profile of PMMA-PnBA-PMMA pattern obtained from PhotoAssist. (**G**) Dielectric constant values as a function of frequency for neat PMMA-PnBA-PMMA elastomer, crosslinked PMMA-PnBA-PMMA elastomer mixed with 10 wt% of linear diazirine crosslinker, and crosslinked film after methyl ethyl ketone development.

Downloaded from https://www.science.org at Institute of High Performance Computing on November 24, 2021

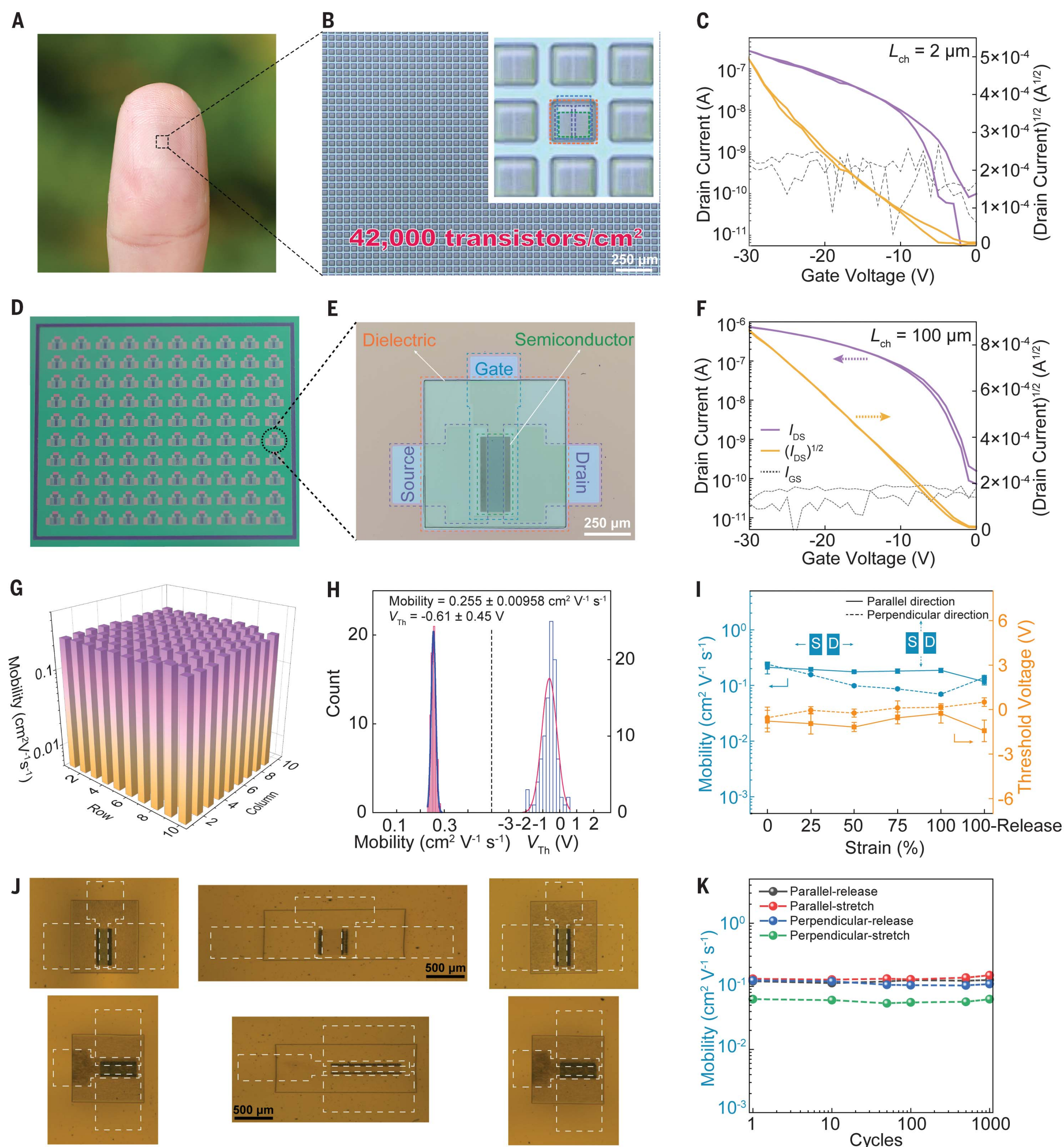

Fig. 4. High-density, highly uniform elastic transistor array fabricated by monolithic optical microlithography. (**A**) An elastic transistor array containing 10,000 transistors attached seamlessly onto the finger. (**B**) Microscope image of the transistor array. Inset: Zoomed-in microscope image of the transistor array (blue dashed line, contour of gate layer; orange dashed line, contour of dielectric layer; green dashed line, contour of semiconductor layer; purple dashed line, contour of source/drain layer). (**C**) Representative transfer curve of a transistor with channel length L_{ch} = 2 μm. (**D**) Photograph of a 10×10 transistor array. (**E**) Microscope image of one transistor from the array with L_{ch} = 100 μm. (**F**) Representative transfer curve of a transistor with L_{ch} = 100 μm. (**G**) Mobility distribution in the 10×10 transistor array. (**H**) Statistical distribution histograms of mobilities (left) and threshold voltage (right) for 98 working devices out of 100 fabricated devices. (**I**) Change of mobility and threshold voltage during stretching up to 100% strain along directions parallel and perpendicular to the charge transport direction. Error bars denote SD. (**J**) Microscope image of a transistor stretched from its original size to 100% strain, then released back to its original size (top, stretched parallel to the charge transport direction; bottom, stretched perpendicular to the charge transport direction). (**K**) Change of mobility under 50% strain and release states during 1000 stretching cycles parallel and perpendicular to the charge transport direction.

Downloaded from https://www.science.org at Institute of High Performance Computing on November 24, 2021

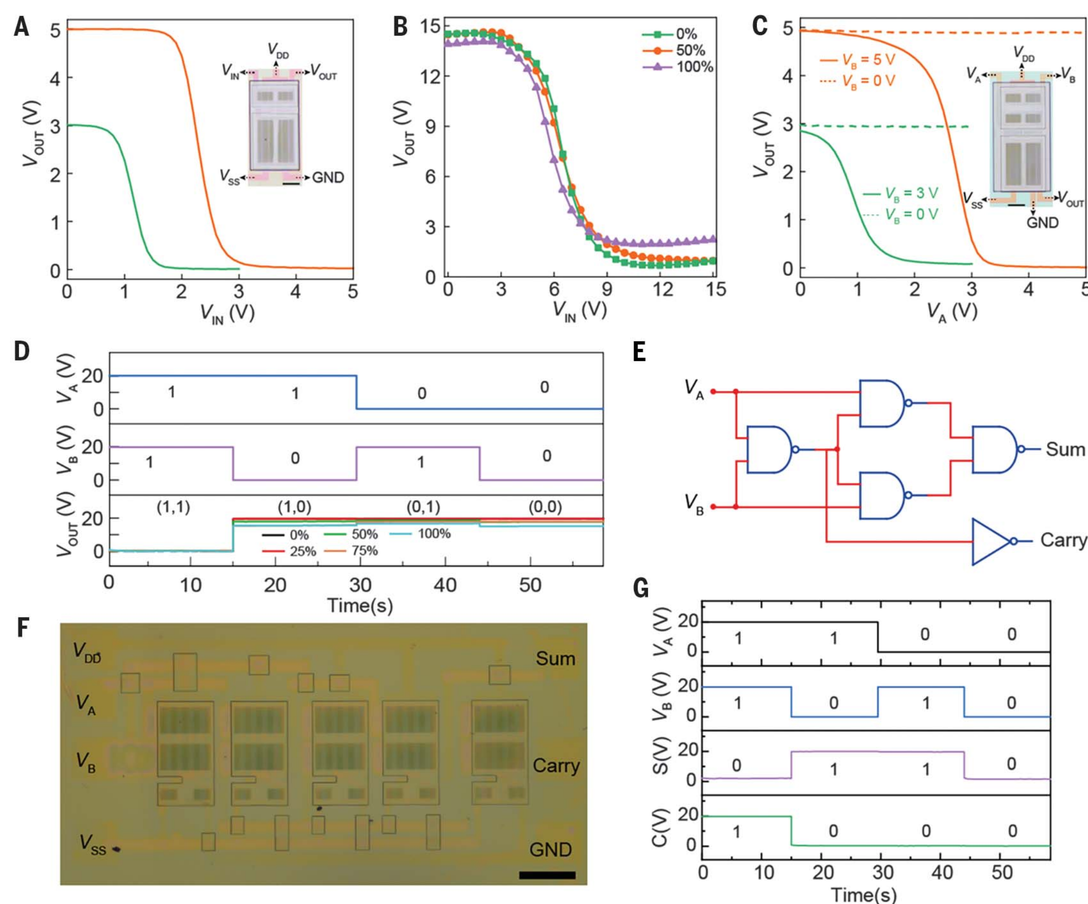

Fig. 5. Elastic functional circuits. (**A**) Transfer characteristics of pseudo-D 10-μm inverter. Inset: Optical image of the inverter. Scale bar, 100 μm. (**B**) Transfer characteristics of pseudo-E 50-μm inverter under strain. (**C**) Transfer characteristics of pseudo-D 10-μm NAND gate. Inset: Optical image of the NAND. Scale bar, 100 μm. (**D**) Output characteristics of pseudo-E 50-μm NAND gate under strain. (**E**) Circuit diagram of a half adder. (**F**) Photograph of a half adder consisting of 30 transistors. Scale bar, 500 μm. (**G**) Output characteristics of the half adder.

Downloaded from https://www.science.org at Institute of High Performance Computing on November 24, 2021

2 μm and channel width W_{ch} of 40 μm. A representative transfer curve of the device indicates typical p-type characteristics, with an on/off ratio of 10^4 and a low off-state current of 0.5 nA (Fig. 4C). Transistors with different channel lengths were fabricated using the PhotoAssist process, and their mobility values showed a dependence on channel length. We observed the highest value of 0.27 $cm^2 V^{-1} s^{-1}$ in a transistor with L_{ch} = 100 μm (figs. S32 and S33). With a decrease in channel length from 100 μm to 5 μm, the increased ratio of contact resistance over channel resistance may result in an underestimation of the charge carrier mobility (fig. S34), which is a common phenomenon for organic semiconductor–based transistors. Therefore, performance for short-L_{ch} elastic transistors can potentially be improved by interfacial modification to achieve better contacts between PEDOT:PSS and semiconducting polymers.

Construction of integrated circuits requires that the elastic transistors be fabricated in a uniform manner and with high yield (*24*). We therefore measured the transfer characteristics of 100 transistors (W_{ch} = 400 μm, L_{ch} = 100 μm) from two different batches of the 10×10 array (Fig. 4, D and E, and figs. S35 and S36). All the transistors showed ideal p-type transfer characteristics with small hysteresis and average saturation mobility of 0.255 $cm^2 V^{-1} s^{-1}$, as extracted from a near-ideal, quadratic current dependence on gate-source voltage (Fig. 4F). In addition, a high device yield of 98.5% and narrow distribution of mobilities with a standard deviation of only 3.76% were achieved (Fig. 4G). The threshold voltage (V_{th}) exhibited a distribution of −0.61 ± 0.45 V (Fig. 4H), a deviation of only 1.5% of the operating gate-source voltage window (−30 V). Minimum variability between transistors is critical for designing complex integrated circuits based on the device modeling and circuit simulation.

The 10×10 transistor array was subjected to 100% strain both parallel and perpendicular to the charge transport direction without any observable cracks or delamination (Fig. 4J), confirming the robust mechanical properties of each layer. The electrical performance of the transistors, including carrier mobilities, threshold voltages, and on-currents, remained stable at <100% applied strain along the charge transport direction, with mobility maintained at 88% of its original value and threshold voltage close to 0 V (Fig. 4I). When the transistors were stretched perpendicular to the charge transport direction, the on-current remained unaffected, with only a slight decrease in mobility (Fig. 4I and fig. S37), which may be due to strain-induced polymer chain alignment (*25*, *26*). Mobility changes in the transistors after being released from parallel stretching may be due to the changes in interface contacts from mechanical mismatches between different layers. The elastic transistors were observed to sustain up to 1000 repeated stretching cycles under 50% mechanical deformation in both directions with negligible changes in mobility (Fig. 4K).

We proceeded to fabricate both inverters and NAND gates, which constitute the basic functional units in elastic digital integrated circuits for on-skin signal processing and computing. Both pseudo-D and pseudo-E inverters with channel lengths ranging from 10 to 100 μm were demonstrated (Fig. 5A and figs. S38 and S39). PhotoAssist allowed fabrication of elastic inverters with channel lengths of 10 μm, which is more than an order of magnitude improvement in spatial resolution relative to previous reports (fig. S40). With its high uniformity and close-to-zero transistor threshold voltage, the pseudo-D 10-μm inverter can be powered by an input voltage of 3 V (Fig. 5A). By varying the input voltage from 0 to 3 V, the output voltage changes from ~3 V to GND. Pseudo-E

50-μm inverters operated normally with logic output states of 1 and 0 under logic input states of 0 and 1, even while being stretched up to 100% strain (Fig. 5B). The excellent uniformity and high yield of the transistors allowed us to build an accurate device model for circuit simulation and optimization to allow the realization of large-scale pseudo–complementary circuits. Simulations based on transistor performance accurately predicted the voltage transfer curves of pseudo-E 50-μm NAND gates (fig. S41). NAND gates consisting of six transistors demonstrated well-defined high- and low-output logic levels as logic "1" and "0" with a low operation voltage down to 3 V (Fig. 5C and fig. S42). Even under 100% strain along the channel length direction, the NAND gate retained the correct output logic (Fig. 5D). More complicated logic circuits—a XOR gate [24 elastic transistors (fig. S43)] and a half adder [30 elastic transistors (Fig. 5E)]—were fabricated (Fig. 5F) and exhibited rail-to-rail outputs (Fig. 5G and fig. S44), indicating that all the elastic transistors worked collectively.

Our PhotoAssist strategy enables direct optical lithography of elastic polymeric electronic materials with micrometer-scale resolution, high yield, and excellent uniformity without compromising their electronic and mechanical characteristics. This work constitutes an increase in elastic-transistor density by more than two orders of magnitude relative to the previously reported highest density (*11*). The general strategy of direct optical patterning of electroactive materials can be extended to both direct laser- and electron beam–writing approaches to further increase the spatial resolution. Additional materials such as biosensing polymers and organic light-emitting materials can also be integrated to construct complex electronic devices.

REFERENCES AND NOTES

1. A. Chortos, J. Liu, Z. Bao, *Nat. Mater.* **15**, 937–950 (2016).
2. Y. Dai, H. Hu, M. Wang, J. Xu, S. Wang, *Nat. Electron.* **4**, 17–29 (2021).
3. S. Lee *et al*., *Science* **370**, 966–970 (2020).
4. S. Sundaram *et al*., *Nature* **569**, 698–702 (2019).
5. T. Araki *et al*., *Adv. Mater.* **32**, e1902684 (2020).
6. J. A. Rogers, T. Someya, Y. Huang, *Science* **327**, 1603–1607 (2010).
7. M. Magliulo *et al*., *J. Mater. Chem. C* **3**, 12347–12363 (2015).
8. Z. Huang *et al*., *Nat. Electron.* **1**, 473–480 (2018).
9. A. D. Valentine *et al*., *Adv. Mater.* **29**, 1703817 (2017).
10. S. Xu *et al*., *Science* **344**, 70–74 (2014).
11. S. Wang *et al*., *Nature* **555**, 83–88 (2018).
12. A. Chortos *et al*., *Adv. Mater.* **28**, 4441–4448 (2016).
13. J. Liang *et al*., *Nat. Commun.* **6**, 7647 (2015).
14. J. F. Chang, M. C. Gwinner, M. Caironi, T. Sakanoue, H. Sirringhaus, *Adv. Funct. Mater.* **20**, 2825–2832 (2010).
15. P. E. Malinowski *et al*., *Org. Electron.* **15**, 2355–2359 (2014).
16. F. Molina-Lopez *et al*., *Nat. Commun.* **10**, 2676 (2019).
17. M. Singh, H. M. Haverinen, P. Dhagat, G. E. Jabbour, *Adv. Mater.* **22**, 673–685 (2010).
18. S. Chung *et al*., *Adv. Mater.* **25**, 4773–4777 (2013).
19. J. Brunner, H. Senn, F. M. Richards, *J. Biol. Chem.* **255**, 3313–3318 (1980).
20. J. Das, *Chem. Rev.* **111**, 4405–4417 (2011).
21. J. Park, M. Koh, J. Y. Koo, S. Lee, S. B. Park, *ACS Chem. Biol.* **11**, 44–52 (2016).
22. S. S. Ge *et al*., *RSC Adv.* **8**, 29428–29454 (2018).
23. G. J. N. Wang *et al*., *Chem. Mater.* **31**, 6465–6475 (2019).
24. L. Xiang *et al*., *ACS Nano* **14**, 6449–6469 (2020).
25. B. O'Connor *et al*., *Adv. Funct. Mater.* **21**, 3697–3705 (2011).
26. X. Zhang *et al*., *Nat. Commun.* **4**, 2238 (2013).

ACKNOWLEDGMENTS

The GIXD measurements were performed at Advanced Light Source beamline 7.3.3 and SSRL 11-3. We thank Y. Ochiai, S. Tatsumi, and Y. Zheng for providing P3HT and DPP polymers. **Funding:** Supported by Stanford Catalyst for Collaborative Solutions. Part of this work was performed at the Stanford Nano Shared Facilities (SNSF), supported by NSF award ECCS-2026822. **Author contributions:** Y.-Q.Z., Y.L., and Z.B. designed the project and experiments; Y.-Q.Z. designed the diazirine crosslinker; Y.-Q.Z. and Y.L. developed the PhotoAssist fabrication method; Y.-Q.Z. and D.Z. fabricated the elastic circuits and carried out electrical characterization; D.Z. carried out the circuit design and simulation; Y.-Q.Z. and Y.L. did the conductivity measurement; Y.-Q.Z., S.L., and D.Z. performed the contact resistance measurement and data analysis; Z.Y. and D.L. synthesized the diazirine crosslinker; S.N. and H.-C.W. carried out GIXD characterization; Y.-Q.Z. and S.N. carried out the 3D profilometer mapping measurement and data analysis; S.L. helped with circuit design; S.N., S.L., and C.Z. helped with device and circuit measurements; J.L. helped to take device photographs; H.T. helped to prepare three-dimensional schematics; Y.-Q.Z., Y.L., Z.B., D.Z., and J.B.-H.T. wrote the manuscript; and all authors reviewed and commented on the manuscript. **Competing interests:** Y.-Q.Z., Y.L., and Z.B. are inventors on a patent application (no. 63/161,344) submitted by the Board of Trustees of Stanford University. **Data and materials availability:** All data are available in the main text or the supplementary materials.

SUPPLEMENTARY MATERIALS

science.sciencemag.org/content/373/6550/88/suppl/DC1
Materials and Methods
Figs. S1 to S43
Tables S1 and S2
References (*27*–*35*)

4 March 2021; accepted 26 May 2021
10.1126/science.abh3551

Downloaded from https://www.science.org at Institute of High Performance Computing on November 24, 2021

Science

Monolithic optical microlithography of high-density elastic circuits

Yu-Qing ZhengYuxin LiuDonglai ZhongShayla NikzadShuhan LiuZhiao YuDeyu LiuHung-Chin WuChenxin ZhuJinxing LiHelen TranJeffrey B.-H. TokZhenan Bao

Science, 373 (6550), • DOI: 10.1126/science.abh3551

Direct optical polymer patterning
As a platform for electronic devices, polymeric materials offer the advantages of intrinsic flexibility and stretchability relative to hard material devices. However, unlike materials such as silicon, there are few tools for large-scale patterning of monolithic devices. Zheng *et al.* developed an optical lithography technique for the high-throughput fabrication of transistor circuitry on stretchable substrates. In this method, ultraviolet light is used to control the local solubility of the polymer, which makes it possible to fabricate transistors on the micrometer scale. These devices can be made with high yield and excellent uniformity without compromising their electronic and mechanical characteristics.

Science, abh3551, this issue p. 88

View the article online
https://www.science.org/doi/10.1126/science.abh3551
Permissions
https://www.science.org/help/reprints-and-permissions

Downloaded from https://www.science.org at Institute of High Performance Computing on November 24, 2021

Use of think article is subject to the Terms of service

Science (ISSN 1095-9203) is published by the American Association for the Advancement of Science. 1200 New York Avenue NW, Washington, DC 20005. The title *Science* is a registered trademark of AAAS.
Copyright © 2021 The Authors, some rights reserved; exclusive licensee American Association for the Advancement of Science. No claim to original U.S. Government Works